Available online at www.sciencedirect.com
SCIENCE DIRECT®
International Journal of Heat and Mass Transfer 48 (2005) 2933–2942
International Journal of HEAT and MASS TRANSFER
www.elsevier.com/locate/ijhmt

Experimental studies on transient features of natural convection in particles suspensions

B. Chen [a,*], F. Mikami [b], N. Nishikawa [b]

[a] Building Environment and New Energy Resource Laboratory, School of Civil and Hydraulic Engineering, Dalian University of Technology, Dalian, Liaoning 116024, PR China
[b] Department of Electronic and Mechanical Engineering, Chiba University, Chiba 263-8522, Japan

Received 26 February 2004; received in revised form 20 September 2004

Abstract

Particle Tracking Velocimetry (PTV), in conjunction with the refractive index matching technique and laser induced fluorescent (LIF) tracer particles, was used to overcome the visualization problem in a particle suspension. A square test section was filled with the particle suspension and impulsively heated from the bottom wall while the two facing vertical walls were kept at a constant temperature. The two-dimensional velocity fields, particle distributions in a plane and the wall temperature fields were visualized simultaneously using three cameras. The results showed peculiar flow patterns such as the formation and vanishing of two-layer convection cells which were distinct from those in a clear, particle-free fluid. Sedimentation driven convection is thought to be the fundamental mechanism for the formation of these two layer convection cells. The overlying particle-free-layer convection was started by the release of the heated clear fluid at the interface between the particle-free layer and the suspension.

1. Introduction

Natural convection in a suspension of small particles occurs in a wide variety of industrial and natural settings, such as solar energy collection system, thermal storage system, suspensions of micro-organisms, to name but a few. In these suspensions, as it is for most of the cases, the suspended particles sediment due to the gravity. This provides the formation of a concentration gradient or density gradient in a suspension which plays an important role in a motion of suspensions. It was noticed by Okada and Suzuki [1] that multi-layer convection cells which were similar to the ones in double-diffusive convection were observed in a fine particle suspension in a rectangular enclosure in which a portion of the lower surface is heated and the two vertical walls are cooled. Another example of such a flow produced in a suspension by the density gradient was investigated in the work of Pedley and Kessler [2] who reported the bio-convection in suspensions of up swimming micro-organisms. The sedimentation of particle suspensions has been extensively studied in recent years [3]. Observation of the flow fields in the suspensions, however, were less successful due to the opacity of the suspensions. We succeeded in visualizing the flow structures of natural convection in suspensions by making the suspensions nearly transparent using refractive index matching technique, where the formation and vanishing of two-layer convection cells were observed [4]. In this study, we have made new

* Corresponding author. Tel.: +86 411 84706371; fax: +86 411 84707273.
E-mail address: chenbin@dlut.edu.cn (B. Chen).

0017-9310/$ - see front matter © 2005 Elsevier Ltd. All rights reserved.
doi:10.1016/j.ijheatmasstransfer.2004.11.016

visual observations of the transient change of convective flows in particle suspensions in order to understand their mechanisms. Attention is focused on the development of convection cells.

2. Visualization in particle suspensions

2.1. Refractive index matching

The refractive index matching technique has been developed as a method for eliminating refraction problems in the optical flow measurements. Many choices of solid and liquid materials for refractive index matching have been studied [5]. Refractive index matching technique has been used in several studies for suspensions to make them optically transparent. Ackerson and Pusey [6] used polymethacrylate (PMMA) particles and refractive index matching fluid of decalin and tetralin mixture to make nearly transparent suspensions for light-scattering study. Another type of materials were used by Nicolai et al. [7] to observe a heavy particle falling in the suspension, where glass beads and a kind of plasticizers were chosen for refractive index matching. In such techniques, the choice of the materials needs special care for dispersion stability and sedimentation rate. In this study, the combinations of fluid and particles were chosen to meet the following criteria. First, the fluid and particles were to have the same index of refraction. Second, the fluid was to be viscous enough for moderate sedimentation rate. Third, the particles were to be dispersed stably in the fluid. The particles chosen were glass beads with index of refraction 1.5. The fluid selected was a mixture of tetralin and silicone oil in proportion (1:2.57, by weight) chosen to nearly match the particle refractive index. Meeting the second criteria was done by choosing the silicone oil with relatively high viscosity (1000 cSt) from the wide variety of products. This combination of fluid and particles satisfied the third criteria. The suspensions were nearly optically transparent as shown in Fig. 1 except for small bubbles in the particle, which allow observation of the tracer particles in the suspension. The details and results of this technique have been described elsewhere [4]. Unfortunately, this technique alone still has the problem, especially in the case of small particle suspensions, that the background scattering noise from suspended particles makes it difficult to separate the tracer particle image from the background and consequently the PTV measurements generate many spurious vectors. To overcome this difficulty, we employed the technique using fluorescent particles described in the next section.

2.2. Laser induced fluorescent tracer particles

The unique feature of the approach described here is the use of fluorescent tracer particles. The basic idea of this approach is to start with polyethylene beads dyed with luminous colors which have the fluorescent capabilities and the favourable properties that they are argon-ion laser excitable.

The removal of the scattering noise was achieved using these fluorescent particles and an optical filter. Since the wave length of emitted fluorescence (λ_2) is longer than that of excitation light (λ_1), we can separate fluorescent image of tracer particles from any scattered excitation light using a sharp cut filter (Fig. 2).

Acrylic polymer emulsion color was found to be the best paint for coating polyethylene beads, because of its strong adhesiveness and water-resistance properties. It is also resistant to the fluid used in this study and never contaminates fluid, which yields clear fluorescent particle image without background fluorescence.

Coating of the polyethylene beads was done as follows. First, mix polyethylene beads and acrylic polymer emulsion color together on the filter paper. After a few minutes of mixing, the particles begin to separate. The final process is the absorbing of the remaining water with filter papers.

Fig. 3a shows polyethylene beads with various acrylic polymer emulsion colors, and their fluorescent image under argon-ion laser light was photographed with the

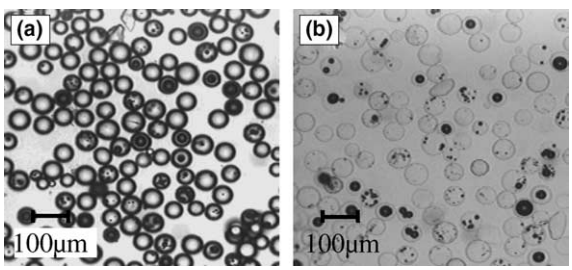

Fig. 1. Photomicrographs of glass beads: (a) with water; (b) with refractive index matching fluid of tetralin and silicone oil mixture.

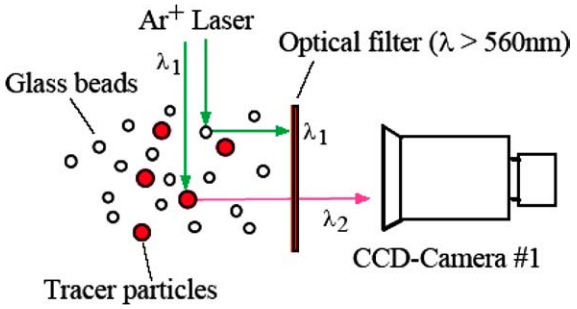

Fig. 2. Laser induced fluorescent particles and function of the optical filter.

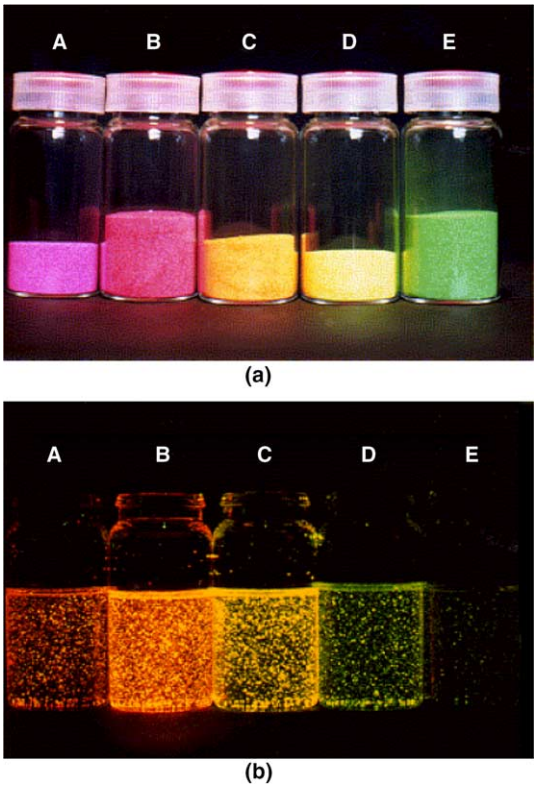

Fig. 3. Tracer particles. (a) Fluorescent color tracer particles. A: luminous rose; B: luminous red; C: luminous orange; D: luminous yellow; E: luminous green. (b) Fluorescent image of tracer particles suspended in tetralin and silicone oil mixture through the optical filter. A ~ E correspond to those in Fig. 3(a).

optical filter. Fig. 3b shows the dependence of the fluorescent colors, from which we chose luminous red as the best color for particle coating.

3. Experiments

3.1. Material

The particles of the suspension are glass beads with index of refraction 1.5, density 2.5 g/cm^3. Measurements by a microscope gave a particle diameter 57.5 μm with a standard deviation 6.4 μm. The distribution of the glass beads diameter is shown in Fig. 4. Glass beads were dispersed in a mixture of tetralin and silicone oil described in the previous section. Physical properties of the suspension and the tracer particles are listed in Table 1.

3.2. Apparatus

Experiments were performed in a square cavity of dimension $L = 60$ mm (60×60 mm square base and 60 mm height). Two vertical cold walls were made of 1 mm copper sheet and held at a constant temperature T_c by circulating the water from a cold bath with thermostat. The bottom surface of the test cell was divided into three segments with the middle 60×30 mm heated section separating two adiabatic sections.

A 10 mm Plexiglas sheet served as the bottom of the test cell. The heated section was installed in a milled groove on the upper face of the sheet so that the top of the heated section was flush with the upper surface of the Plexiglas sheet. The heater consisted of a 1 mm copper top plate and an electric sheet heater (20 V–30 W). A thermocouple was installed below the copper plate, and its output was monitored by an electronic control circuit which adjusted the power to the heater so as to maintain temperature of the copper plate to $T_h \pm 0.1$ °C. Other thermally insulating walls were made of 10 mm Plexiglas sheet. A schematic of the test cell is shown in Fig. 5.

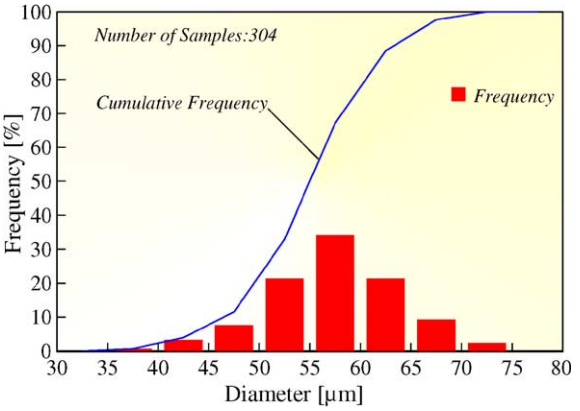

Fig. 4. Distribution of glass beads diameter.

Table 1
Physical properties of the particles, suspending fluid and tracer particles used in the experiments

Glass beads	
Density	2.5 g/cm^3
Average radius	57.5 ± 6.4 μm
Suspending fluid	
Density	0.975 g/cm^3
Viscosity (at 30 °C)	20.12 cSt
Refractive index	1.50
Thermal diffusivity	5.35×10^{-8} m^2/s
Thermal expansion Coefficient	0.7996×10^{-3} 1/K
Tracer particles	
Density	0.975 g/cm^3
Average radius	161.5 ± 17.9 μm

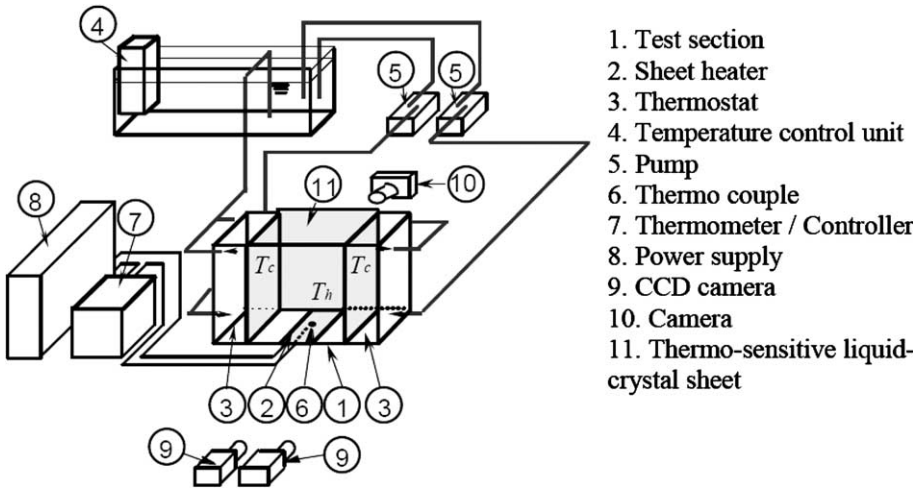

Fig. 5. Scheme of the experimental setup.

The test section was filled with a suspension held at the uniform temperature T_c prior to application of bottom heating. The suspension was mixed well by a rod and kept still for 30 s to minimize perturbation when it was judged to be uniformly mixed. Transient flow is initiated by impulsively increasing the temperature of the hot wall to T_h.

3.3. Measurements

Figs. 6 and 7 show the principle of the visualization method and the measurement system, respectively. The suspension was seeded with the small amount of fluorescent tracer particles (0.37 g/l), and the fluorescence emission from these particles were captured by the CCD-Camera #1 under a vertical argon-ion laser light sheet (approximately 1.5 mm thick). An optical filter ($\lambda > 560$ nm) separates emitted fluorescence from scattered excitation light, and thus clear tracer particle images without any scattering noise from suspended particles were obtained. The laser light sheet was synchronized with the TV signal with 10 ms emission period using AOM to obtain an instant image within a frame. The captured images were recorded on a VCR #1. The triple pattern matching method [8] was used here for particle tracking between video frames. The slow nature

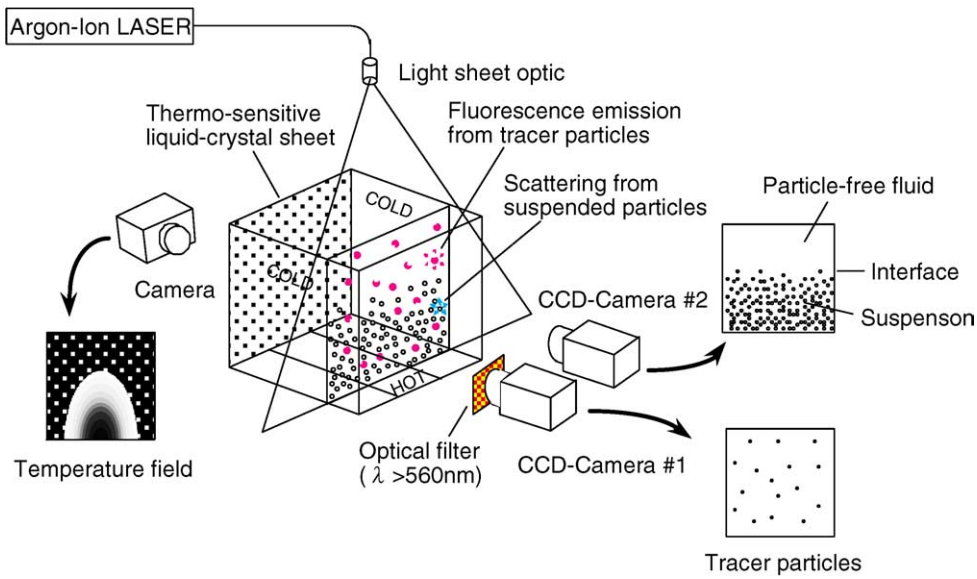

Fig. 6. Principle of the visualization method.

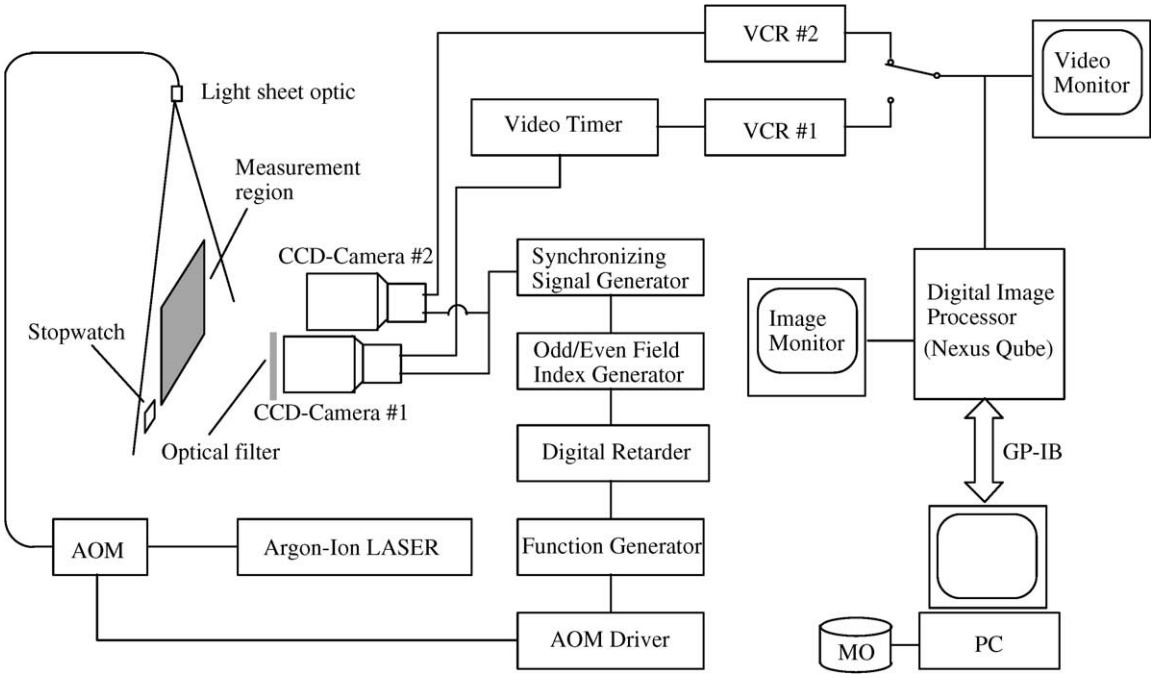

Fig. 7. Measurement system.

of convective flows makes it difficult to obtain velocity vectors from contiguous video frames. The following results are based on the video sampling at a rate of 1 frame per second.

The CCD-Camera #2 detects the scattering light image of suspended particles under the same laser light sheet which yields the information of particle distributions in the plane. The suspension layer and the particle free layer were estimated based on the difference of light intensity. The captured images were recorded on a VCR #2.The wall temperature fields were visualized with the thermo-sensitive liquid crystal sheet film having the working ranges from 30 to 35 °C. The reaction of the sheet to the environment temperature yields colormaps which were photographed under lighting of a halogen l amp.

Velocity and particle distributions were measured at a location $z = 5L/6$ in the suspension. Fig. 8 shows the velocity distributions in various planes in the test section obtained by the PTV for steady state convection with $\phi =$ 0 wt%, $\Delta T = 15°C$ which ensures two dimensionality of the convective flows. It may be admitted that flow fields at a location $z = 5L/6$ represent the whole flow fields in the cell.

Table 2 lists the parameters of the experiments. In this study, temperature difference ΔT was kept constant and ϕ was varied. In this dilute conditions, the heat transfer associated with the sedimentation of particles is thought to be negligible.

4. Results and discussion

4.1. Transient change of flow patterns

Typical flow visualization results are shown in Figs. 9 and 10 for clear particle-free fluid and 3 wt% suspension, respectively. These pictures are generated by 20 video frames of CCD-Camera #1 with sampling rate of 2 frames per second. Fluorescent images of tracer particles yield clear streak lines and improved the sharpness of pictures compared with non-fluorescent particles in our previous study [4].

A pair of convection cells was observed all the time for the particle-free fluid as seen in the Fig. 9. While in a suspension, peculiar flow patterns which were distinct from those in a particle free fluid were observed as shown in Fig. 10, where convective flow patterns changes with time accompanied by the formation and vanishing of the two-layer convection cells.

It is helpful to organise a description of the development of the convection cells into a number of stages. This can be done as follows [4].

Stage 1. In this stage, convective motion is induced by bottom heating and the vertical propagation of the convection cell is suppressed by the formation of a particle-free layer at the top.

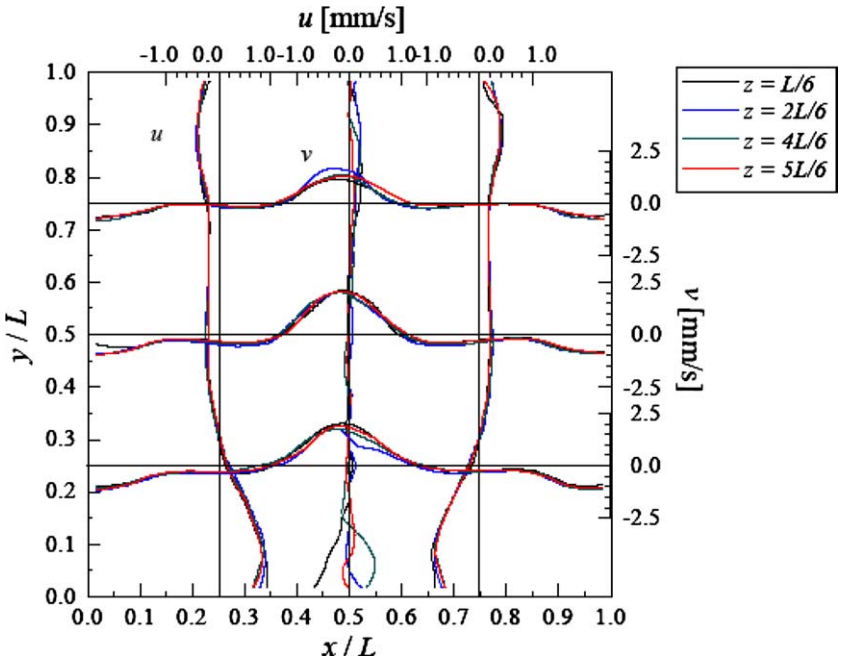

Fig. 8. Velocity profiles in various planes for steady state convection with $\phi = 0$ wt%, $\Delta T = 15$ °C.

Table 2
The parameters in experiments

ΔT (°C)	15
T_h (°C)	43
T_c (°C)	28
Grashof number, *Gr*	5.81×10^4
Prandtl number, *Pr*	2.40×10^2
Rayleigh number, *Ra*	1.42×10^7
Particle concentration, ϕ	
(wt%)	0, 3
(volume fraction)	0, 0.0116

Stage 2. During the second stage, upperlayer convection is initiated, and two-layer double convection cells are observed.

Stage 3. The next stage is characterized by the development of upper-layer convection in size with a growing layer of clear particlefree fluid at the top.

Stage 4. The forth stage is characterized by the transition from two-layer convection to single-layer convection with upper convection cells reaching the bottom surface.

Stage 5. During the fifth stage, we encounter the breakdown of the interface between particle-free layer and suspension with lifted heavy suspension becoming unstable. This leads to chaotic motion of the fluid.

Stage 6. In the final stage, most of the suspended particles settle down, and steady single cell convection pattern similar to that of particle-free fluid is observed.

4.2. Flow fields, particle distributions, and wall temperatures

In this section, we describe the simultaneous measurements of the velocity fields, particle distributions, and wall temperatures. A primary purpose of the measurements was to reveal the mechanism of the formation and vanishing of the two-layer convection cells in a suspension. In order to get some idea of the interaction between particle- and temperature distributions, we made a synthesized image of velocity fields, particle distributions and the temperature fronts. Fig. 11 shows the procedure for the image processing.

Velocity vectors obtained by PTV were grid interpolated from which flow structures can be visualised. The images of the particle distributions were enhanced by changing the brightness into pseudo color maps with the red and green regions showing the suspension layer and the clear particle free fluid, respectively. Temperature front which separates the heated region (at least 2 °C above T_c) from another was traced as a border of red color region in the thermo-sensitive liquid-crystal sheet which approximately indicates 30 °C isotherm.

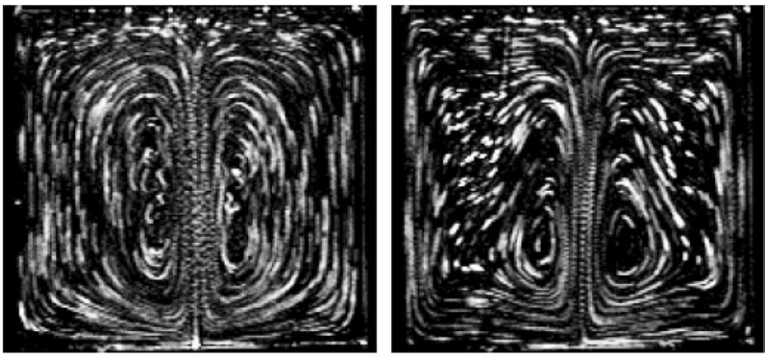

Fig. 9. Flow patterns at (a) 60 s and (b) 1200 s after initiation with $\phi = 0$ wt%, $\Delta T = 15$ °C.

Again we describe the evolution of the convection cells with these synthesized images (Fig. 12a–h). The fluid was almost quiescent just after the initiation as shown in Fig. 12a, where particle-free layer began to appear at the top. In Stage 1 (Fig. 12b), the convection started in the bottom of the suspension layer while the particle-free layer was still quiescent. At the end of the Stage 1 as shown in Fig. 12c, vertical propagation of the convection and the temperature were suppressed by the upper particle-free layer. Fig. 12d illustrates the beginning of the Stage 2 during which upper-layer convection starts. The location of the temperature fronts were almost same in Fig. 12c and d, while the location of the interface in Fig. 12d is lower than that in Fig. 12c due to the sedimentation of the particles. The fluid at the interface convected into the upper layer and carried with it some of the particles to form mushroom-like distribution of the suspended particles (Fig. 12e: Stage

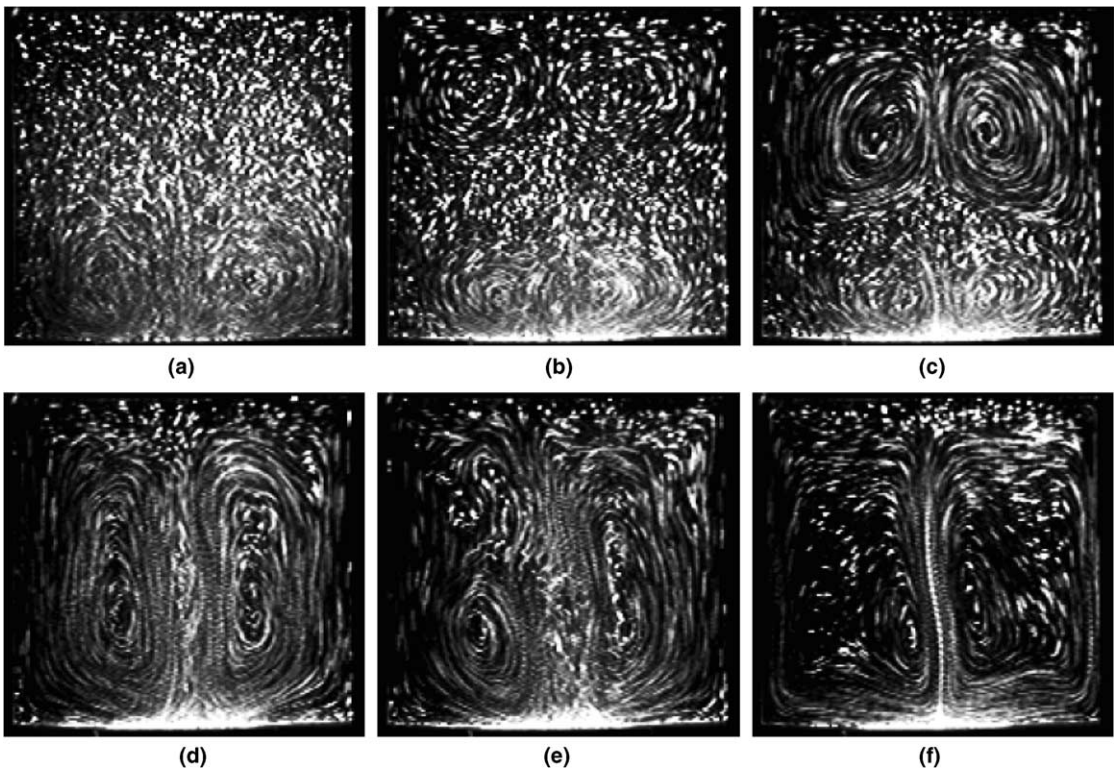

Fig. 10. Typical stages of the development of convection cells with $\phi = 3$ wt%, $\Delta T = 15$ °C. (a) 35 s, Stage 1; (b) 185 s, Stage 2; (c) 250 s, Stage 3; (d) 335 s, Stage 4; (e) 375 s, Stage 5; (f) 1200 s, Stage 6.

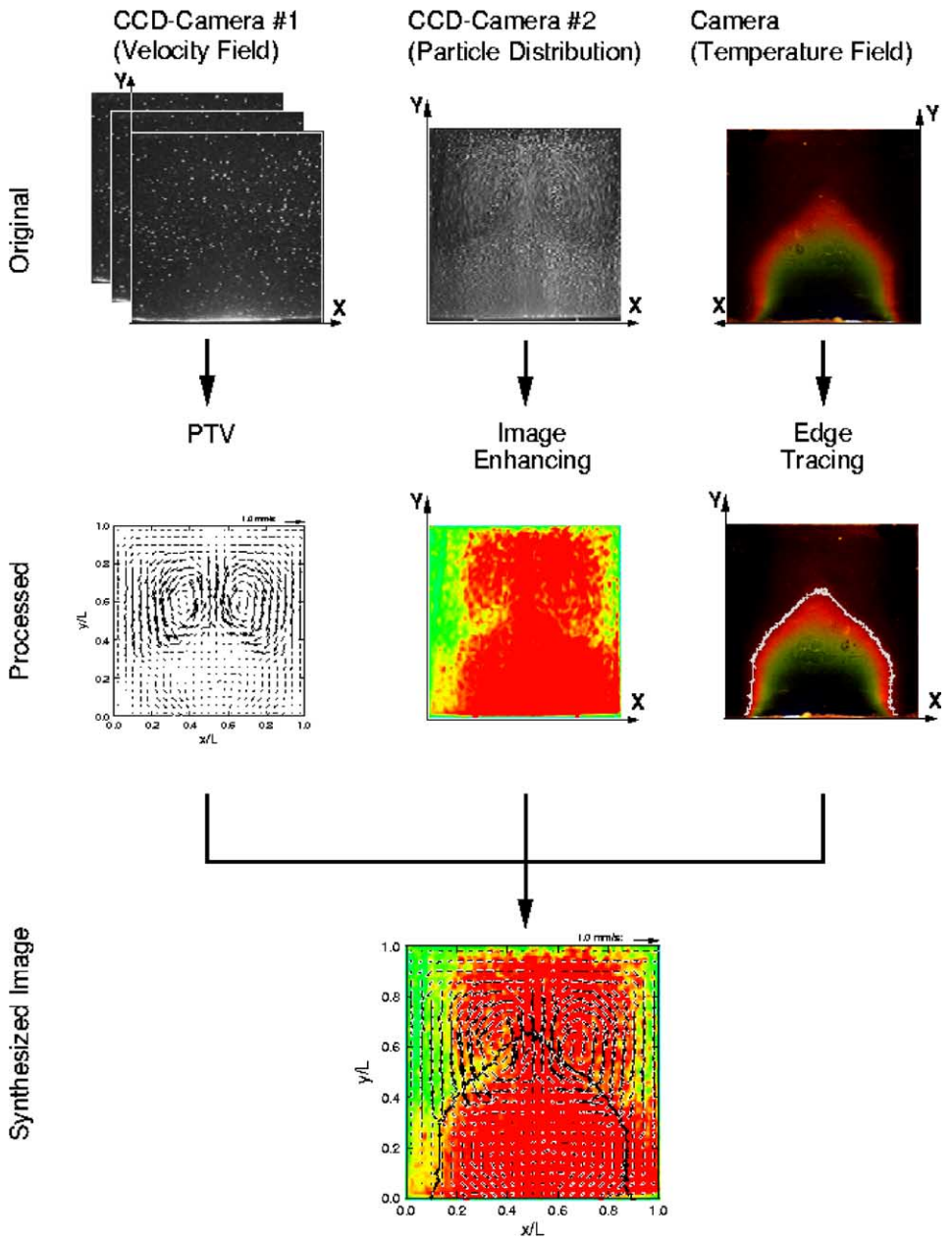

Fig. 11. The procedure for image processing.

3). The upper-layer convection cell developed in size with a growing layer of clear particle-free fluid at the top and the transition from two-layer convection to single layer convection occurred producing suspension column (Fig. 12f: Stage 4). This lifted heavy suspension became unstable and interfacial breakdown occurred accompanied by the chaotic motion of the fluid (Fig. 12g: Stage 5). After the breakdown, most of the particles settled down and steady convection cell forms in the cavity (Fig. 12h: Stage 6).

4.3. Explanation of the occurrence of two-layer convection cells

As described in the previous two sections, there is a complex phenomenology associated with the evolution of convection cells. This includes the suppression of the vertical propagation of the convection, the formation of two-layer double convection cells, the growth of upper-layer convection, the instability of lifted suspension and interfacial breakdown. Here we discuss

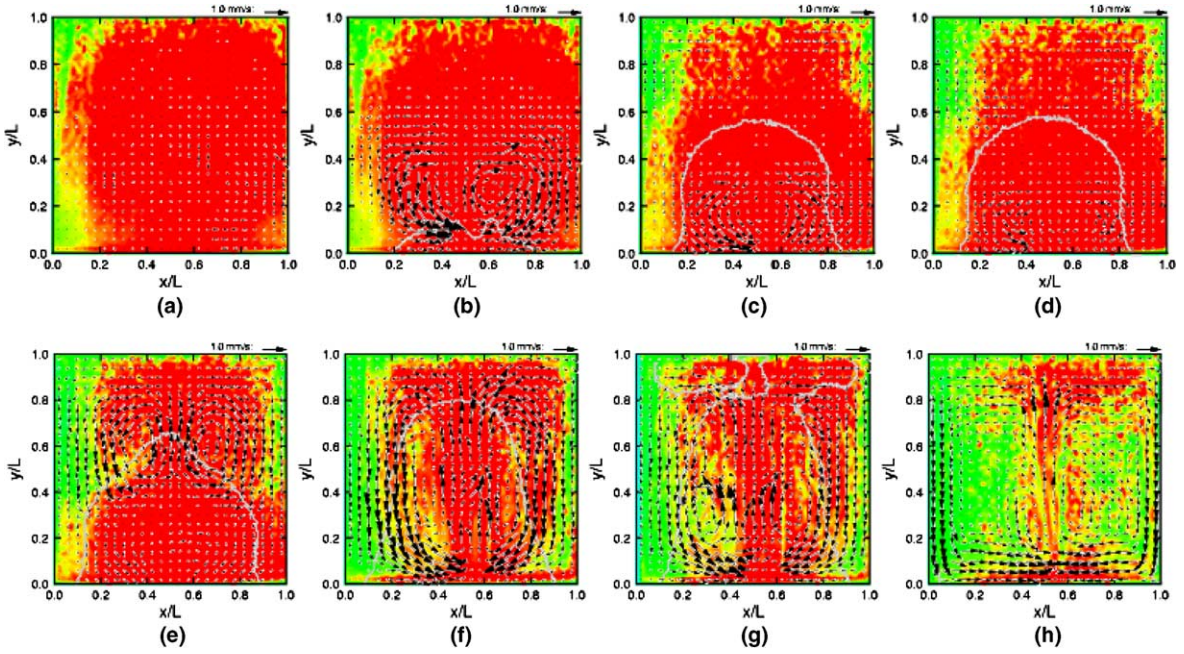

Fig. 12. Transient change of flow patterns, particle distributions, and temperature fronts after initiation. (a) 0 s; (b) 35 s; (c) 165 s; (d) 185 s; (e) 250 s; (f) 335 s; (g) 375 s; and (h) 1200 s.

some attempts to make explanation of the formation of two-layer double convection cells from our visualization results.

In seeking an explanation of the formation of two-layer convection cells, we begin with the transient change of the location of the top surfaces of the suspension layer and the temperature front. The sedimentation curves in Fig. 13 show the time courses of the vertical location of the interface between particle-free layer and suspension at the left and the right walls. While the rising curves in Fig. 13 show the temperature front for the 3 wt% suspension and particle-free fluid, which separate the upper cold region and the lower heated region. The temperature front curve for 3 wt% suspension has a plateau beginning at about 80 s and ending at about 250 s after initiation showing the suppression of the vertical heat transfer associated with the convective flow patterns. In contrast, plateau did not appear in the particle-free fluid. It must be noticed that the time at which upper-layer convective motion started coincides with the time when the sedimentation curve crosses the temperature front curve.

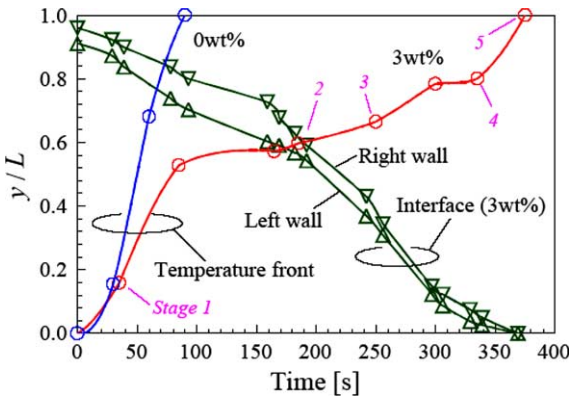

Fig. 13. Time courses of the temperature front and interface location. Stages 1–5 correspond to those in Fig. 10.

It is possible at this point to make a comparison of the above observations of the condition for the formation of the upper-layer convection cell with the study of Huppert et al. [9] on systems for a suspension of small particles overlain by a clear fluid whose density is greater than that of the interstitial fluid, but less than that of the bulk suspension. They reported that the settling of the suspended particles in the lower layer can lead to convection in the overlying particle-free fluid releasing light fluid convecting into the upper layer. It is likely that the same situation occurs in this study; the overlying particle-free layer convection is initiated by the release of the heated clear fluid at the interface.

Fig. 14 illustrates the mechanism for the formation of two-layer convection cells. The density of the liquid is given, as a function of both temperature and volume fraction of the particles, by a linear equation of state of the form

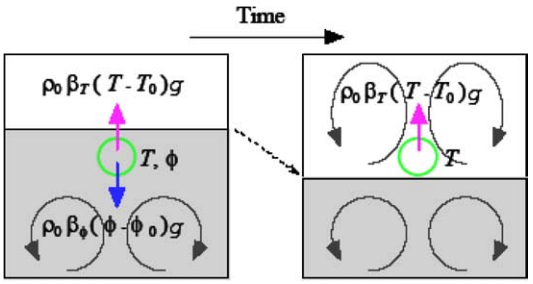

Fig. 14. Sedimentation driven convection.

$$\rho = \rho_0\{1 - \beta_T(T - T_0) + \beta_\phi(\phi - \phi_0)\}$$

T and ϕ denote temperature and volume fraction of the particles, respectively, and the subscripts 0 denote reference values. Just before the sedimentation curve crosses the temperature front, the buoyant force $\rho_0\beta_T(T - T_0)g$ is balancing with the negative buoyant force $\rho_0\beta_\phi(\phi - \phi_0)g$ at a region near the interface. When the interface pass through the temperature front, the volume fraction at the concerned region changes from certain positive value to zero vanishing the negative buoyant force, and consequent upper-layer convection starts at that time. It may be admitted now that this fundamental mechanism, sedimentation driven convection, can be attributed to the formation of two-layer convection cells.

5. Conclusions

The visualization method presented here has been shown to provide satisfactory results for the problems of natural convection in particle suspensions. The particle tracking velocimetry, in conjunction with the refractive index matching technique and laser induced fluorescent tracer particles, has enabled the quantitative velocity measurements in a suspension. The development of the convective flows in a suspension were clarified with simultaneous measurements of velocity, particle, and temperature distributions. We may conclude that the observed two-layer convection cells were driven by the sedimentation of particles which releases the heated clear fluid at the interface.

References

[1] M. Okada, T. Suzuki, Natural convection of water-fine particle suspension in a rectangular cell, Int. J. Heat Mass Transfer 40 (1997) 3201–3208.
[2] T.J. Pedley, J.O. Kessler, Hydrodynamic phenomena in suspensions of swimming microorganisms, Ann. Rev. Fluid Mech. 24 (1992) 313–358.
[3] R.H. Davis, A. Acrivos, Sedimentation of noncolloidal particles at low Reynolds numbers, Ann. Rev. Fluid Mech. 17 (1985) 91–118.
[4] F. Mikami, B. Chen, N. Nishikawa, Visualization of the flow features of natural convection in particle suspensions, Theor. Appl. Mech. 46 (1997) 341–348.
[5] R. Budwig, Refractive index matching methods for liquid flow investigations, Exp. Fluids 17 (1994) 350–355.
[6] B.J. Ackerson, P.N. Pusey, Shear-induced order in suspensions of hard spheres, Phys. Rev. Lett. 61 (1988) 1033–1036.
[7] H. Nicolai, Y. Peysson, É. Guazzelli, Velocity fluctuations of a heavy sphere falling through a sedimenting suspension, Phys. Fluids 8 (1996) 855–862.
[8] K. Nishino, K. Torii, A fluid-dynamically optimum particle tracking method for 2-D PTV: triple pattern matching algorithm, Proc. ISTP-6 in Thermal Eng. 3 (1993) 339–344.
[9] H.E. Huppert, R.C. Kerr, J.R. Lister, J.S. Turner, Convection and particle entrainment driven by differential sedimentation, J. Fluid Mech. 226 (1991) 349–369.